AGU ADVANCING EARTH AND SPACE SCIENCE

JGR Oceans

Key Points:
- The ^{14}C levels in DOC and DIC of the South China Sea are equal to the levels in the western and central North Pacific
- The South China Sea is largely influenced by the Kuroshio Current extrusion
- The distribution and cycling of DIC and DOC in the deep South China Sea are largely controlled by hydrodynamic processes

Radiocarbon in Dissolved Organic and Inorganic Carbon of the South China Sea

Ling Ding[1], Yuanzhi Qi[1], Sen Shan[1], Tiantian Ge[1], Chunle Luo[1], and Xuchen Wang[1,2] (iD)

[1]Key Laboratory of Marine Chemistry Theory and Technology, Ministry of Education/Center for Frontier Science of Deep Ocean and Earth System, Ocean University of China, Qingdao, China, [2]Center for Isotope Geochemistry and Geochronology, Qingdao National Laboratory for Marine Science and Technology, Qingdao, China

Abstract We present the carbon isotope (^{14}C and ^{13}C), dissolved inorganic carbon (DIC), and dissolved organic carbon (DOC) concentration measurements in the South China Sea (SCS) to reveal the different sources and cycling time scales of the two major carbon pools in the SCS. The DIC concentrations ranged from 1,776 to 2,328 μmol kg^{-1}, and they were lower at the surface and increased with depth. Conversely, the DOC concentrations ranged from 38 to 95 μM, and they were higher on the surface and decreased rapidly in the upper 500-m water depth. The DIC Δ^{14}C and DOC Δ^{14}C values varied from -227‰ to 68‰ and -557‰ to -258‰, respectively, and both decreased with depth until 1,500 m and then remained relatively constant. DOC Δ^{14}C values were -330‰ lower than DIC Δ^{14}C, indicating that DOC has cycled for much longer than DIC in the SCS. The lower Δ^{14}C-DIC and Δ^{14}C-DOC values at depths shallower than 700 m were mainly influenced by intensified vertical mixing, which upwelled the deep water with low Δ^{14}C-DIC and Δ^{14}C-DOC values for thorough mixture with the upper layer water. Conversely, the small difference in the Δ^{14}C signature in deep water ($>1,500$ m) between the SCS and the North Pacific confirmed the rapid water exchange through the Luzon Strait and rapid water mixing in the SCS basin, which plays an important role in controlling carbon cycling in the deep SCS.

Plain Language Summary Dissolved inorganic carbon (DIC) is the largest carbon pool in the ocean and is closely linked to dissolved organic carbon (DOC), which is the largest exchangeable organic carbon pool in the ocean. Both DIC and DOC play important roles in the global carbon cycle, but their sources, distribution, and cycling time are different and controlled by different processes in the ocean. Here we report radiocarbon and stable carbon isotope measurements of DIC and DOC collected in the South China Sea (SCS) to reveal the sources and cycling time scales of the two major carbon pools in the SCS. The Δ^{14}C values and ^{14}C ages indicate that DOC has cycled for much longer than DIC in the SCS. The rapid water exchange and mixing between the SCS and the Kuroshio Current in the Northwestern Pacific play important roles in controlling the distributions and cycling of DIC and DOC in the SCS.

1. Introduction

Dissolved inorganic carbon (DIC) and dissolved organic carbon (DOC) represent two major but well-linked carbon pools in the ocean, and both play important roles in the global carbon cycle (Hansell et al., 2009; Key, 1996). The distribution and dynamics of DIC and DOC in the ocean are modulated not only by anthropogenic CO_2 invasion and biological processes but also by changes in physical processes and ocean circulation (Bercovici & Hansell, 2016; Carlson et al., 2010; Gruber, 2011; Hansell et al., 2009; Wakita et al., 2010; Winn et al., 1998). Radiocarbon measurements of dissolved carbon (both DIC and DOC) have provided valuable information on the sources and cycling time scales of each carbon pool (Druffel et al., 1992, 2008; Key et al., 1996; McNichol et al., 2000; McNichol & Aluwihare, 2007; Williams & Druffel, 1987). Studies have revealed that DIC and DOC have very different ^{14}C ages in the ocean, which is related to the mechanisms and processes controlling the sources and cycling of DIC and DOC. The DIC ages in the North Atlantic and North Pacific (NP) were found to be 650 and 2,000 ^{14}C years old, and the DOC ages in the North Atlantic and NP were found to be 4,000 and 6,000 ^{14}C years old, respectively. The older ages of DIC and DOC indicate much longer cycling time scales in the NP than in the North Atlantic (Druffel et al., 1992, 2008; Key et al., 1996; McNichol et al., 2000; Williams & Druffel, 1987). The vastly different ^{14}C ages of DIC and DOC in the deep North Atlantic and NP oceans have been largely attributed to the time scale of the deep ocean conveyor (Broecker et al., 1985; Druffel & Griffin, 2015; Key et al., 2004; Stuiver et al.,

1983). However, the much older DOC than DIC (3,300–4,000 years) in the deep ocean remains an unsolved mystery of the carbon cycle in the ocean (Druffel et al., 2016; Follett et al., 2014).

The South China Sea (SCS) is a semienclosed marginal sea in the western Pacific Ocean with a total area of 3.5×10^6 km^2 (Figure 1). The average water depth of the SCS is 1,210 m, and the deepest water depth in the basin reaches 5,300 m. The SCS has a wide shelf (150–300 km) and slope in its northern part covering a surface area of more than 1.2×10^6 km^2 and is connected to the East China Sea through the shallow Taiwan Strait. The northern shelf region of the SCS is influenced by the input of the Pearl River, the third longest river (~2,200 km) in China, which discharges approximately 3.3×10^{11} m^3 of freshwater annually into the SCS (Dai et al., 2014). The Luzon Strait, located at the northeastern rim with a maximal sill depth of ~2,400 m, is the only deep channel that connects the SCS with the western Philippine Sea in the Northwestern Pacific (NWP); this connection allows for water exchange between the SCS and the NWP (Liu et al., 2008; Qu et al., 2006; Shu et al., 2014; Tian & Qu, 2012; Wang et al., 2016).

Several studies have been conducted to assess the carbon cycle in the SCS, including both the DIC and DOC pools (Cao et al., 2011; Dai et al., 2009, 2013; Hung et al., 2007; Wu et al., 2015). Few records of water DIC ^{14}C have been documented in the SCS. Gao et al. (2019) recently suggested that the spatial variations in Δ^{14}C-DIC values in the surface water of the SCS were mainly due to lateral mixing between the SCS and NWP. The only four intermediate-deep depth seawater Δ^{14}C-DIC data points measured in the central SCS basin showed a rapid deep-water exchange between the two basins (Broecker et al., 1986). Furthermore, the exchange of DOC between the SCS and open ocean would also have important implications for the DOC dynamics in the ocean interior, with an estimated 3.1 ± 2.1 Tg C year^{-1} of DOC exported to the adjacent open ocean through the Luzon Strait (Dai et al., 2009; Wu et al., 2015). However, no records of water DOC ^{14}C have been documented, and thus, the ^{14}C ages of DOC in the SCS are unknown.

Here we report radiocarbon (^{14}C) and stable carbon (^{13}C) isotope values measured for the whole water column of six stations in the SCS and two stations in the eastern Luzon Strait. These new results provide useful information on the carbon cycles, water exchange processes, and circulation processes in the SCS.

2. Methods

2.1. Study Site and Sample Collection

Water samples used for DIC and DOC analyses were collected from eight stations in the SCS and in the eastern region of the Luzon Strait (Figure 1) during three cruises. Water samples from stations S1, S2, and S3 were collected on R/V *Shiyan 3* during 11–20 July 2015, and water samples from stations A11, D2, and K2 were collected on R/V *Dongfanghong 2* during 11–24 May 2016. Samples from stations C05 and C08 were collected on R/V *Science* in July–August 2019. General information on the sampling stations is provided in supporting information Table S1. Stations C05 and C08 from the eastern Luzon Strait are located in the main path of the Kuroshio Current in the NWP. Station D2 is in the northern slope region of the SCS, and the water depth is 1,700 m. Other stations (S1, S2, S3, A11, and K2) are in the SCS basin, and the water depth ranges from 2,800 (S1) to 4,300 m (S3) (Figure 1).

Water samples were collected using 12 L Niskin bottles attached to a rosette sampler with conductivity, temperature, and depth sensors that recorded the temperature and salinity profiles. For DIC water collection, we used the protocol described in McNichol and Jones (McNichol & Jones, 1991). Water was collected (after overflowing ~100 ml) into prebaked 100 ml glass bottles with fine-ground glass stoppers using precleaned silicone tubing connected directly to the Niskin bottle and immediately treated with 50 μl of saturated HgCl$_2$ solution. Then, the bottles were capped tightly with grease-coated, ground glass stoppers and secured with rubber bands to make a gas-tight seal to avoid CO$_2$ exchange with the atmosphere. All DIC samples were kept in the dark at room temperature. DOC samples were transferred directly from the Niskin bottles into a 1 L precleaned and combusted (at 550 °C for 4 hr) glass bottle after rinsing three times with seawater. The water was immediately filtered onboard through prebaked (at 550 °C for 4 hr) 47 mm Whatman GF/F filters (0.7 μm pore size). Then, the filtered seawater was acidified with superhigh-purity 85% H$_3$PO$_4$ to pH = 2 and frozen at −20 °C until analyses could be conducted.
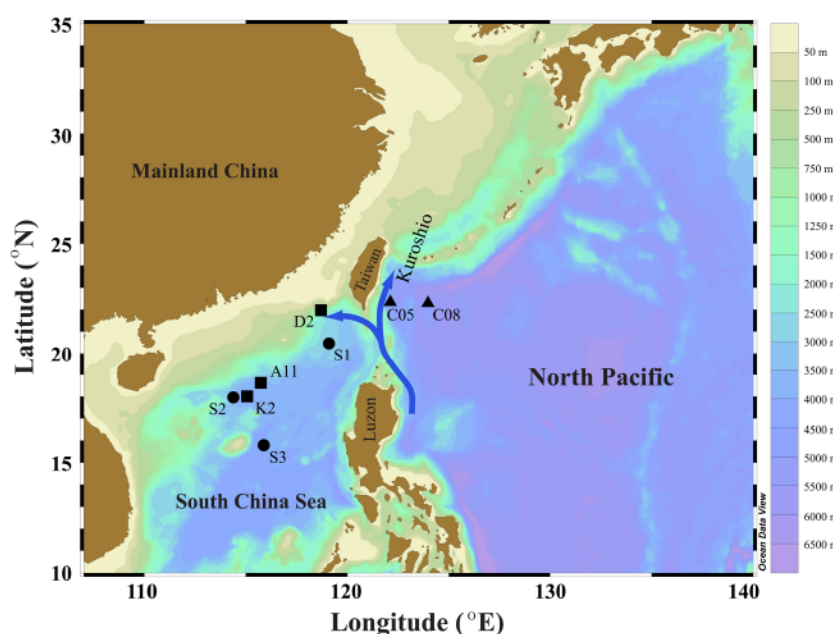
Figure 1. Map of the South China Sea (SCS) and the Northwestern Pacific. The sampling locations from the three SCS cruises in June–July 2015 (black circles), May–June 2016 (black squares), and July–August 2019 (black triangles) are also shown. The blue arrows indicate the northward-flowing Kuroshio Current as the major western boundary current of the North Pacific and its branch into the SCS. The map was created with ODV (Schlitzer, 2017).

2.2. DIC and DOC Concentration Analyses

DIC and DOC concentrations were measured using a Shimadzu TOC-L analyzer equipped with an ASI-V autosampler. DIC concentrations were analyzed using the total inorganic carbon mode and calibrated using a six-point standard calibration curve prepared from reagent grade sodium carbonate and sodium bicarbonate dissolved in Milli-Q water. The instrument blank and DIC values were checked against DIC reference materials (CRMs supplied by Dr. A. Dickson at Scripps Institution of Oceanography). The total blanks associated with DIC measurements were less than 3.0 μM, which is approximately <0.15% of the seawater DIC concentrations, and the analytic precision of triplicate injections was <2%.

Concentrations of DOC were analyzed by the high-temperature catalytic oxidation method (Sharp et al., 1995). DOC concentrations were calibrated using a six-point standard curve generated by using DOC standard solutions prepared from potassium hydrogen phthalate and UV-oxidized purity Milli-Q water. The running blank was determined using high-purity Milli-Q water that was analyzed between samples. The quality assessment involved verification against low-carbon water and deep seawater (CRM Batch 13 with 41–44 μM DOC concentration) references provided by the Hansell Biogeochemical Laboratory at the University of Miami. The average blank associated with DOC measurements was ≤5 μM, and the coefficient of variation for the analysis of the triplicate injections was approximately 3%. All samples were analyzed in duplicate from different vials, and the standard deviations of the replicate measurements ranged from ±0.1 to 4.0 μM.

2.3. DIC and DOC Isotopic Measurements

DIC samples were processed in the laboratory within 2 weeks after each cruise. DIC was extracted as gaseous CO_2 using our modified method (Ge et al., 2016) based on McNichol et al. (1994), with an extraction efficiency >96%. Briefly, in a N_2-filled glove box, a 50 ml water sample was injected into a preevacuated 100 ml borosilicate glass bottle with ground glass joint stripping probes. After the injection of 1.0 ml of 85% H_3PO_4 using a glass syringe and stainless steel needle, the glass bottle with the acidified water sample was placed in a hot water bath (70 °C) for 30 min and shaken by hand several times. At pH ≤ 2, all forms of DIC (carbonate, bicarbonate, and CO_2) dissolved in water become CO_2. At 70 °C under vacuum, the solubility of CO_2 in water is calculated to be $<6.0 \times 10^{-5}$ μmol L^{-1}, and it is expected that all CO_2 dissolved in water
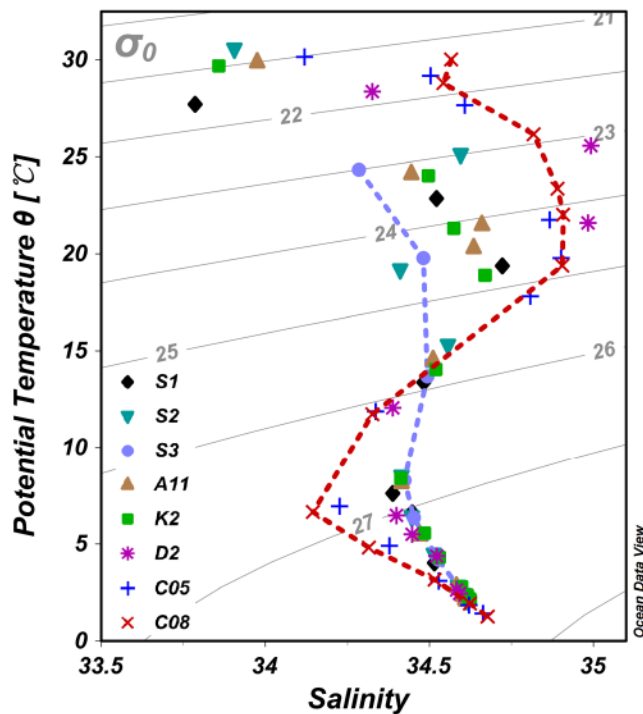
Figure 2. Potential temperature versus salinity (T-S) diagram for the sampling stations in the SCS and the NWP. Isopycnals (σ_0) are included in the diagram. The colored symbols correspond to conductivity, temperature, and depth data, and the dashed lines denote typical SCS water (S3) and typical Kuroshio water (C08) from the three cruises during 2015–2019.

has escaped into the probe headspace. The glass bottle was removed from the hot water bath, cooled for 5 min, and then connected to the vacuum line. All extracted CO_2 was frozen into a liquid nitrogen trap. After measuring and recording the volume, the purified CO_2 was flame-sealed inside 6 mm OD Pyrex tubes for ^{14}C and ^{13}C analyses.

For DOC ^{14}C and ^{13}C measurements, DOC was first oxidized using the modified UV-oxidation method (Xue et al., 2015). Briefly, ca. 500 ml of filtered and acidified seawater was placed into a series connection of custom-made 100 ml quartz reaction tubes specifically designed to interface directly with a vacuum extraction line. Water samples were first purged with ultrahigh-purity helium gas for 40 min to remove DIC and then irradiated using a 1.2 kW medium-pressure mercury arc UV lamp (Hanovia Co.) for 5 hr. Following UV irradiation, the CO_2 evolved from DOC was purged again with ultrahigh-purity helium gas through the vacuum line and cryogenically stripped. The purified CO_2 was flame-sealed inside 6 mm OD Pyrex tubes for ^{13}C and ^{14}C analyses. The oxidation efficiency and blanks associated with the UV-oxidation of DOC were tested using high-purity Milli-Q water and a DOC standard (oxalic acid) solution, yielding a high oxidation efficiency (~95%) of DOC and reasonable low blanks (<4 μgC). The blank level was approximately <2% of the typically collected sample size (~220 μgC).

Both $\delta^{13}C$ and $\Delta^{14}C$ measurements were performed at the National Ocean Sciences Accelerator Mass Spectrometry (NOSAMS) facility at the Woods Hole Oceanographic Institution (WHOI) and at the Center for Isotope Geochemistry and Geochronology (CIGG) at the Qingdao National Laboratory for Mari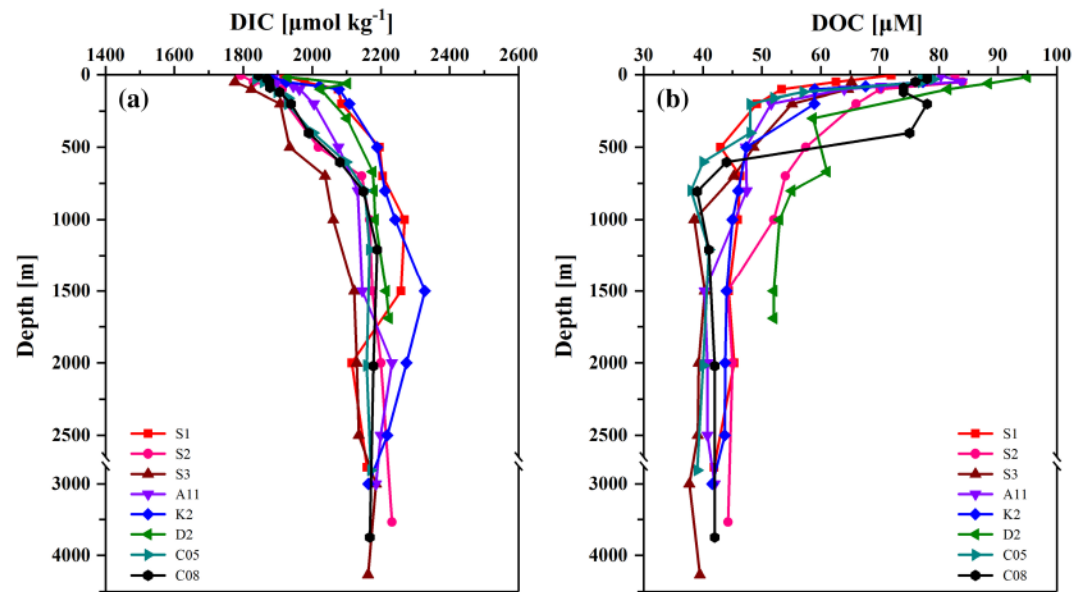ne Science and Technology (QNLM) in Qingdao, China. Purified CO_2 samples were graphitized for ^{14}C analysis using AMS. The $\Delta^{14}C$ results were reported as fraction modern (McNichol et al., 1994), and the conventional radiocarbon ages (years before present) were calculated using the Libby half-life as described by Stuiver and Polach (1977). The total uncertainties of the $\Delta^{14}C$ measurements are ±4.0‰ and ±6.0‰ for DIC and DOC, respectively. The $\delta^{13}C$ value of each DOC sample was measured on a small split of CO_2 that was produced from UV-oxidized DOC using a Thermo 253 Plus Isotope Ratio Mass Spectrometer (IRMS). For $\delta^{13}C$-DIC measurements, a water sample (1.5 ml) was transferred into a 30 ml prevacuumed LABCO vial and automatically analyzed using a Thermo Delta-V IRMS coupled with a Thermo Gasbench II system at CIGG. The $\delta^{13}C$ values are reported in ‰ relative to the VPDB standard for DIC with a total uncertainty of ≤0.2‰, and IAEA standards (IAEA-CH$_3$ Cellulose and IAEA-600 Caffeine) for DOC with a total uncertainty of ±0.6‰.

3. Results

3.1. Hydrography

All the hydrographic data on temperature and salinity are summarized in Table S2. The temperature exhibited highly constant and similar profiles through the water column for eight stations, even though water samples were collected from different cruises in three different years (July 2015, May 2016, and July–August 2019) (Figure S1). Water temperature decreased rapidly from the surface down to 1,500 m (~30.5 to ~ 2.9 °C) and then remained constant below 1,500 m at density levels of $\sigma_0 \geq 27.6$ (Figures S1 and 2). The salinity ranged from 33.786 to 34.993 and exhibited different depth-profile patterns from that of temperature for the eight stations (Figure S1). As shown in the temperature-salinity (T-S) diagram (Figure 2), the overall hydrographic properties showed an inverse "S" shape with different curved patterns. Salinity increased rapidly with depth to reach a maximum at the density range of 23.0–24.9 σ_0 (50–200 m water depth) and subsequently decreased to a minimum of approximately 600 m (density σ_0 ~ 26.8). The salinity at all stations remained relatively uniform at deeper depths (below 1,500 m) with a density layer of $\sigma_0 \geq 27.6$ (Figures 2 and S1). While the salinity maximum was reached at depths of approximately

Figure 3. Depth profiles of DIC and DOC concentrations measured at the eight stations in the SCS and NWP during the three cruises in 2015–2019. Note that the depth below 2,500 m is on a different scale.

50–200 m (23.0–24.9 σ_0) at all stations, this maximum was much less pronounced at the SCS basin stations S1, S2, S3, A11, and K2 than at the other three stations (stations D2, C05, and C08); thus, less curved patterns of T-S distributions were observed in the SCS basin (i.e., stations S1, S2, S3, A11, and K2) than in the eastern Luzon Strait (i.e., stations C05 and C08) (Figure 2, red dashed line).

3.2. Concentrations and Distributions of DIC and DOC

The DIC concentrations ranged from 1,776–2,328 µmol kg^{-1} (Table S2) and were lower in the surface layer (≤5 m depth) and increased with depth for all stations (Figure 3a). DIC concentrations were higher at stations S1 and K2 but lower at S3 in the upper 1,500 m depth. Below a depth of 1,500 m, the concentrations of DIC remained less variable for each station. The DOC concentrations were highest in the surface 100 m of water depth (53–95 µM, Figure 3b and Table S2) and decreased rapidly to 500 m across all stations, then remained constant in the range of 38–45 µM in deep waters (approximately below 1,500 m depth except station D2). The average DOC values below 1,500 m for most stations (except station D2) ranged from 39 to 44 µM. The DOC concentrations at slope station D2 were significantly higher than those at most stations in the upper 1,700 m water depth, and station S3 in the central basin had the lowest DOC concentrations (38–40 µM).

3.3. Isotopic Distributions of DIC and DOC

The Δ^{14}C and δ^{13}C results for both DIC and DOC are listed in Table S2, and depth profiles are presented in Figure 4. The Δ^{14}C-DIC values ranged from −227‰ to 68‰ with high values in the upper 100 m water depth and decreased rapidly down to 1,500 m, although the trend exhibited some variations among the eight stations (Figure 4a). The most variability in Δ^{14}C-DIC was observed between 200 and 1,500 m depth, where higher Δ^{14}C-DIC values were seen for samples at stations C05 and C08 in the NWP, with a range of 24‰ to 68‰ in the upper 500 m depth. However, between 500 and 1,500 m depth, the Δ^{14}C-DIC values at station S1 (−216‰ to −110‰) were generally lower than those at other stations. The Δ^{14}C-DIC profiles for the other five stations (S2, S3, A11, K2, and D2) showed a high degree of similarity (Figure 4a). The δ^{13}C-DIC values ranged from −0.61‰ to 0.72‰, and the values decreased rapidly in the upper 200 m depth for all stations (Figure 4b). The δ^{13}C-DIC values were less variable below 500 m with the exception of two high values (0.05‰ and 0.22 ‰) at station C08.

The Δ^{14}C and δ^{13}C values of DOC were measured only for samples collected from four stations (S1, S2, S3, and A11). The Δ^{14}C-DOC values were generally much lower than the Δ^{14}C-DIC values, by −330‰,
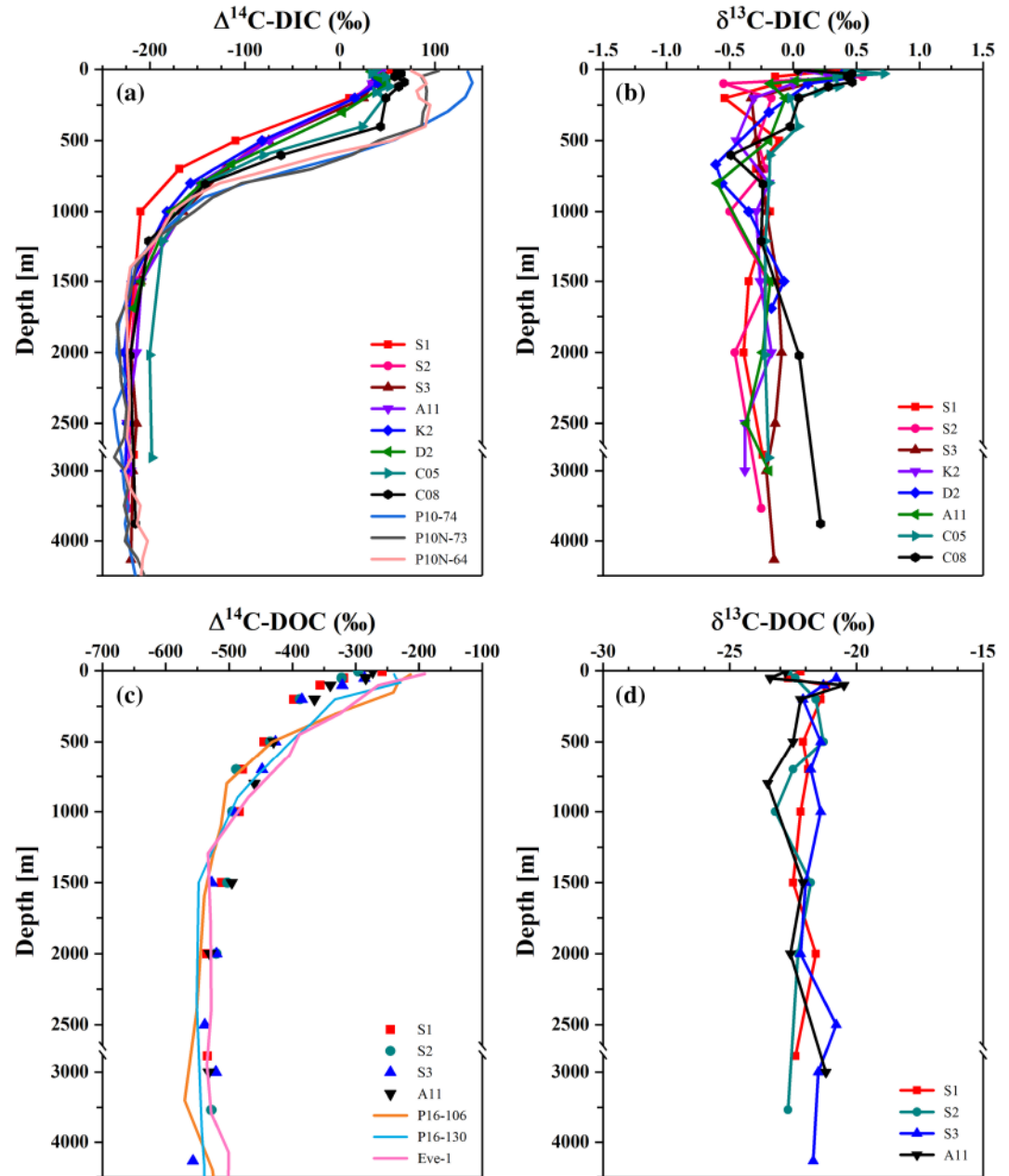
Figure 4. Depth profiles of (a) Δ^{14}C-DIC, (b) δ^{13}C-DIC, (c) Δ^{14}C-DOC, and (d) δ^{13}C-DOC measured at the eight stations in the SCS and NWP during three cruises in 2015–2019. Note that the depth below 2,500 m is on a different scale. The following Δ^{14}C-DIC and Δ^{14}C-DOC values are also shown for comparison with the results in this paper: (a) the Northwestern Pacific stations P10-74 (28.5°N 149.3°E) in 1993, P10N-73 (29.2°N 149.3°E) and P10N-64 (22.5°N 149.4°E) in 2005 (Fukasawa et al., 2005; Key, 1996; Key et al., 2002); and (c) the central North Pacific stations Eve-1 (31°N 159°W) in 1987, P16-106 (19°N 152°W) and P16-130 (31°N 152°W) in 2015 (Druffel et al., 1992, 2019).

and ranged from −557‰ to −258‰ (Table S2). However, the Δ^{14}C-DOC profiles for the four stations exhibited a similar pattern to those of Δ^{14}C-DIC, i.e., higher values at the surface decreased quickly with depth and then remained relatively constant below a water depth of 1,500 m (Figure 4c). The lowest value (−557‰) was found in the central basin deep water (4,267 m) at station S3. The δ^{13}C-DOC values ranged from −20.5‰ to −23.5‰ with no obvious systematic variations with depth for each station (Figure 4d).

4. Discussion

4.1. Profiles of Δ^{14}C-DIC: Implications for Water Mixing Dynamics in the SCS

The Δ^{14}C-DIC and DIC concentrations have been used as conservative tracers of water mass movement and water parcel homogenization in the ocean (Beaupré & Aluwihare, 2010; Ding et al., 2018; Key et al., 1996). The majority of DIC in the surface ocean (0–100 m) is from atmospheric CO_2 entering the ocean through air-sea exchange and dissolved as carbonate species. The Δ^{14}C-DIC values in the surface ocean thus reflect the atmospheric bomb ^{14}C signals, and the values subsequently decrease with depth as a consequence of deep water isolation from the atmosphere and net radiocarbon decay (Druffel et al., 2016). The Δ^{14}C-DIC profiles measured for all stations both in the SCS and east of the Luzon Strait clearly reflect this trend (Figure 4a). The average Δ^{14}C-DIC value (45‰) in the surface 50 m in the SCS was lower than the surface Δ^{14}C-DIC values (135‰ for P10-74 and 88‰ on average for P10N-64 and P10N-73) at three earlier stations (see details in Figure 4a) in the NWP. As reported by previous studies, the global average Δ^{14}C value in atmospheric CO_2 has decreased from ~150‰ in 1990 to ~31‰ in 2012 (Hua et al., 2013; Levin et al., 2013), which could account for the surface Δ^{14}C-DIC differences between our sites and the three earlier P10-Line stations. Although the bomb ^{14}C signals have been well mixed into the upper 1,500 m depth of the water column in the SCS and the east of Luzon Strait (Figure 4a), the upper ocean has now become a source of bomb ^{14}C and is capable of transferring ^{14}C back to the atmosphere (Gao et al., 2019).

Considering the T-S diagram (Figure 2) and Δ^{14}C-DIC profiles (Figure 4a), the water below 1,500 m depth in the SCS basin was well mixed during sampling. The observed salinity and Δ^{14}C-DIC variations appeared only in the upper 1,500 m depth. As one of the largest semienclosed marginal seas with a deep basin in the tropical NWP, the surface circulation in the SCS is driven mainly by the influences of strong seasonal monsoons (Hu et al., 2000; Liu et al., 2008; Su, 2004). The lower surface salinity at the five stations in the SCS basin than at the stations (C05 and C08) in the east of the Luzon Strait (Figures 2 and S1) is attributed to precipitation exceeding evaporation in the SCS (Wang & Li, 2009). The Luzon Strait is the only deep channel for water movement and exchange between the SCS and NWP (Figure 1) (Liu et al., 2008; Shu et al., 2014; Tian & Qu, 2012; Wang et al., 2016). The Kuroshio, which is the major western boundary current of the subtropical NWP, flows northward along the coast of Luzon, and a fraction of the Kuroshio water passes through the Luzon Strait and enters the SCS (Liu et al., 2008). Studies have shown that the vertical water transport through the Luzon Strait exhibits a sandwiched three-layer structure with a net inward flow in the upper (0–500 m) and deep (>1,500 m) layers and a net outflow in the middle layer (500–1,500 m) (Liu et al., 2008; Shu et al., 2014; Tian et al., 2006). It is believed that the vertical motion induced by strong diffusive mixing could be the primary mechanism driving deep circulation and meridional overturning circulation in the SCS (Lan et al., 2013; Shu et al., 2014; Tian et al., 2009; Wang et al., 2016). Our Δ^{14}C-DIC profiles of the eight stations seem to support this mechanism, confirming that water was well mixed deep (>1,500 m) in the basin of the SCS during different sampling periods. Another important clue is the very small difference in Δ^{14}C-DIC values in the deep water below 1,500 m between the SCS and NWP, implying rapid water exchange through the Luzon Strait.

To examine the influence of the intrusion of the Kuroshio water mass into the SCS, we compared the Δ^{14}C-DIC profiles in the upper 1,300 m depth at two stations (S1 and S3) in the SCS basin with a station (C08) located in the path of the northward-flowing Kuroshio Current east of the Luzon Strait. As shown in Figure 5, Δ^{14}C-DIC values at 500 m in the SCS were −100‰ to −150‰ lower than Kuroshio water at the same depth. In the Kuroshio path in the NWP, water was well mixed with the surface bomb ^{14}C signals down to 500 m, below which radiocarbon values decreased rapidly with depth. However, in the SCS, this high surface atmospheric bomb ^{14}C signal (~50‰) was observed only in the upper 100 m and then diluted rapidly with deep low-Δ^{14}C water (Figures 4a and 5). This large variation in Δ^{14}C-DIC values between the SCS stations and NWP station in the upper water column cannot be explained by the decreased air-sea ^{14}C gradient (Gao et al., 2019; Graven et al., 2012). Hence, the differences between the SCS and Kuroshio reflect the different water masses and mixing dynamics. Compared with the Kuroshio water, it was likely that the lower Δ^{14}C-DIC values in the upper 250–700 m depth inside the SCS were not influenced by the upper layer (0–500 m) of the Kuroshio Current that intruded into the SCS through the Luzon Strait, but by the intermediate or deep water masses of the NWP. As evidence, station S1 is located in the middle of the Luzon Strait entrance and could be directly influenced by the Kuroshio water intrusion. However, the Δ^{14}C-DIC
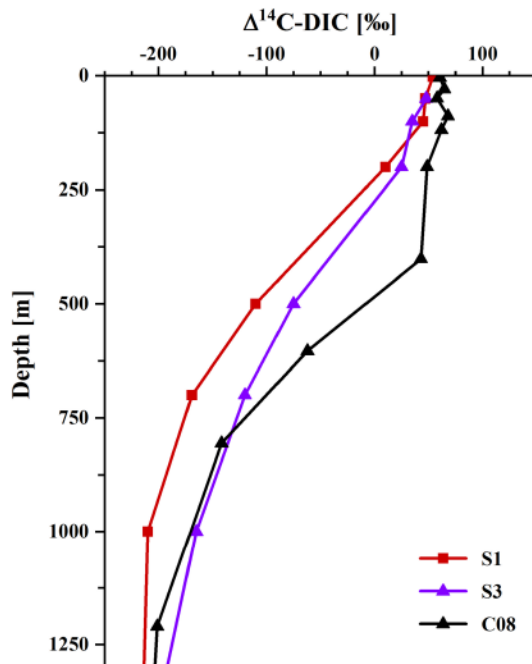
Figure 5. The Δ^{14}C-DIC values (‰) versus water depth (m) measured in the upper 1,300 m at stations S1, S3, and C08 in the SCS and NWP.

values of S1 were significantly lower (by ~30–150‰) than those of the other stations in the depth range of 300–1,300 m (Figure 5). The influence of the Kuroshio and vertical mixing process are demonstrated more clearly in Figure 6, which plots the longitudinal cross-section distributions of salinity, DIC concentrations, and Δ^{14}C-DIC values for the five stations (K2, A11, S1, C05, and C08) from west to east across the Luzon Strait. Combined with the T-S diagram (Figure 2), the cross-section salinity plot (Figure 6a) showed that the water characteristics in the SCS have reduced extreme salinity signals and less curved inverse "S" shapes than those in the eastern Luzon Strait due to upwelling and enhanced vertical mixing in the SCS interior (Cao et al., 2011; Dai et al., 2009; Tian et al., 2009). Physical oceanographic studies have reported that the abyssal basin of the SCS is filled by deep NWP water flowing down the sill of the Luzon Strait (Chen et al., 2001; Gong et al., 1992), and the deep SCS water is believed to upwell into intermediate depths between 350 and 1,350 m (Chen & Huang, 1996; Su, 2004). It is likely that the deep NP water with low Δ^{14}C-DIC values upwelled and mixed with the surface water, thus reducing the observed Δ^{14}C-DIC profiles for the stations in the upper 250–700 m in the SCS. However, it appears that intensive upwelling and vertical mixing are relatively strong in the Luzon Strait (Tian et al., 2009), resulting in much higher DIC concentrations and lower Δ^{14}C-DIC values in the upper 250–1,000 m, as shown in Figures 6b and 6c.

4.2. DOC and Δ^{14}C-DOC in the SCS

Concentrations and distribution of DOC in the SCS showed typical DOC vertical patterns in the ocean with accumulated DOC in the upper layer of the water column and relatively constant values below 1,000 m water depth, reflecting DOC production in the euphotic zone and microbial consumption with depth (Carlson et al., 1994; Hansell et al., 2009; Hansell & Carlson, 2001, 2013). The DOC concentrations (average 75 ± 8 μM) in the upper layer (0–100 m) during the spring and summer seasons were comparable to the values previously reported by Dai et al. (2009) and recently reported by Wu et al. (2015) for the SCS. The Kuroshio intrusion was the dominant factor in enhancing the DOC contents in the SCS during spring (Wu et al., 2015). The elevated DOC levels at northern slope station D2 could have been influenced by the stronger intrusion of the Kuroshio Current and high primary production in spring. However, this intrusion was weaker in summer and decreased with distance from the Luzon Strait (Du et al., 2013; Nan et al., 2015), resulting in DOC concentrations that were not significantly elevated at other stations in the SCS basin. The newly produced DOC was labile and rapidly remineralized in the euphotic zone, leaving the refractory fraction of DOC to cycle in the deep water (Carlson et al., 2010; Hansell & Carlson, 2013).

The Δ^{14}C-DOC values in the upper 1,000 m of the water column were higher (Table S2) and contained bomb ^{14}C, which was fixed into organic matter during photosynthesis. Although the general shapes of the Δ^{14}C-DOC and Δ^{14}C-DIC profiles are similar (Figures 4a and 4c), there is a consistent offset between the two profiles with lower Δ^{14}C-DOC values, corresponding to DOC ^{14}C ages approximately 3,900 ± 248 years older on average, similar to the age differences between the DOC and DIC pools in the oceans (Druffel et al., 2016; Druffel & Bauer, 2000). Comparing the SCS Δ^{14}C-DOC with the values reported previously in the central NP (Figure 4c) showed lower Δ^{14}C-DOC values (−322‰ to −258‰) in the SCS water shallower than 250 m because of intense vertical mixing of the deep waters that upwelled to the surface in this marginal sea, bringing lower Δ^{14}C waters to the surface. In contrast, higher Δ^{14}C-DOC values (greater than −250‰) were found on the surface of the subtropical Pacific, where downwelling is dominant (Druffel et al., 2019). The relatively constant Δ^{14}C-DOC values for samples below 1,500 m in the SCS were similar to those from the central NP, with averages that were nearly equal within an acceptable error range (−525 ± 15‰ and −533 ± 17‰, respectively) (Figure 4c). No significant aging of the DOC can be seen for deep water in the SCS basin, suggesting that DOC has been transported with the inflow from the NWP as it traveled across the Luzon Strait and well mixed into the deep water. Additionally, δ^{13}C-DOC values in
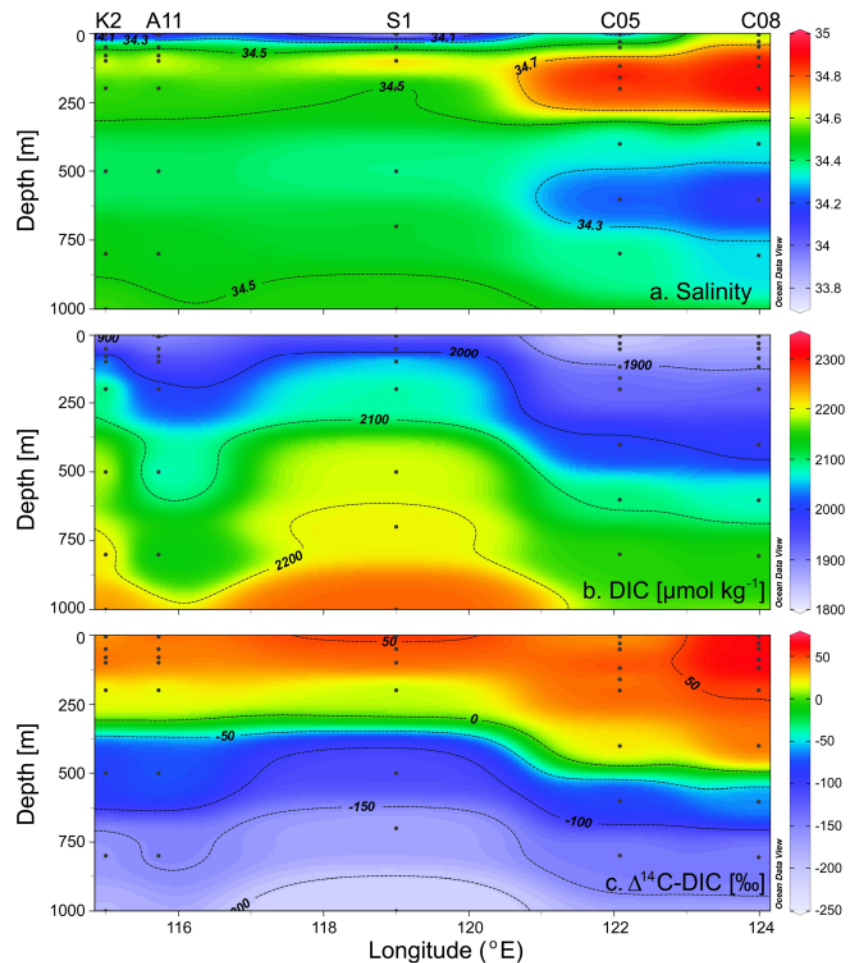
Figure 6. Distribution of (a) salinity, (b) DIC concentrations, and (c) Δ^{14}C-DIC values of the water samples collected from five stations during three cruises in 2015–2019 using Ocean Data View (Schlitzer, 2017).

the SCS ranged between −20.5‰ and −23.5‰, consistent with the values reported recently for DOC in the ocean (Druffel et al., 2019; Zigah et al., 2017), suggesting that DOC cycling in the deep ocean could derive from mixed marine, terrestrial, and hydrothermal sources (Follett et al., 2014; Zigah et al., 2017). The surface circulation gyres affected by the strong monsoon have effectively isolated the SCS basin from the influence of land runoff in a wide oligotrophic area, such as the interior of the major ocean basins (Gong et al., 1992; Hu et al., 2000; Liu et al., 2008). This finding supports the Δ^{14}C-DOC profiles discussed above, where intense diffusive and vertical mixing could be the main factors controlling the distributions of DOC and Δ^{14}C-DOC in the SCS.

The positive relationship of DOC concentration and Δ^{14}C-DOC ($R^2 = 0.79$, $p < 0.001$ in Figure 7b) for the stations further suggested that vertical mixing could describe mass and isotope balances of DOC between surface and deep waters. In our study, if surface DOC in the SCS was comprised of a mixture of deep DOC below 1,500 m depth (42 ± 3 µM and −525 ± 15‰ on average, respectively) and modern surface-produced DOC (74–42 = 32 µM with an average Δ^{14}C-DOC nearly equal to surface Δ^{14}C-DIC value of 44‰), then the total surface DOC (74 µM) would have a Δ^{14}C value of −279‰ in the SCS. This calculated value agrees with the average measured Δ^{14}C-DOC values (−291‰) in the upper 50 m (Figure 4c). Furthermore, there was a significant correlation ($R^2 = 0.93$, $p < 0.001$) between the Δ^{14}C-DOC and Δ^{14}C-DIC values obtained from water in the same Niskin bottles at the four stations in the SCS (Figure 7c). The parallel profiles and significant correlation suggest that DIC and DOC Δ^{14}C are tightly coupled throughout the entire water column, and a common process would influence both carbon pools, as shown previously using data from the central NP (Beaupré & Druffel, 2009; Druffel et al., 2019).
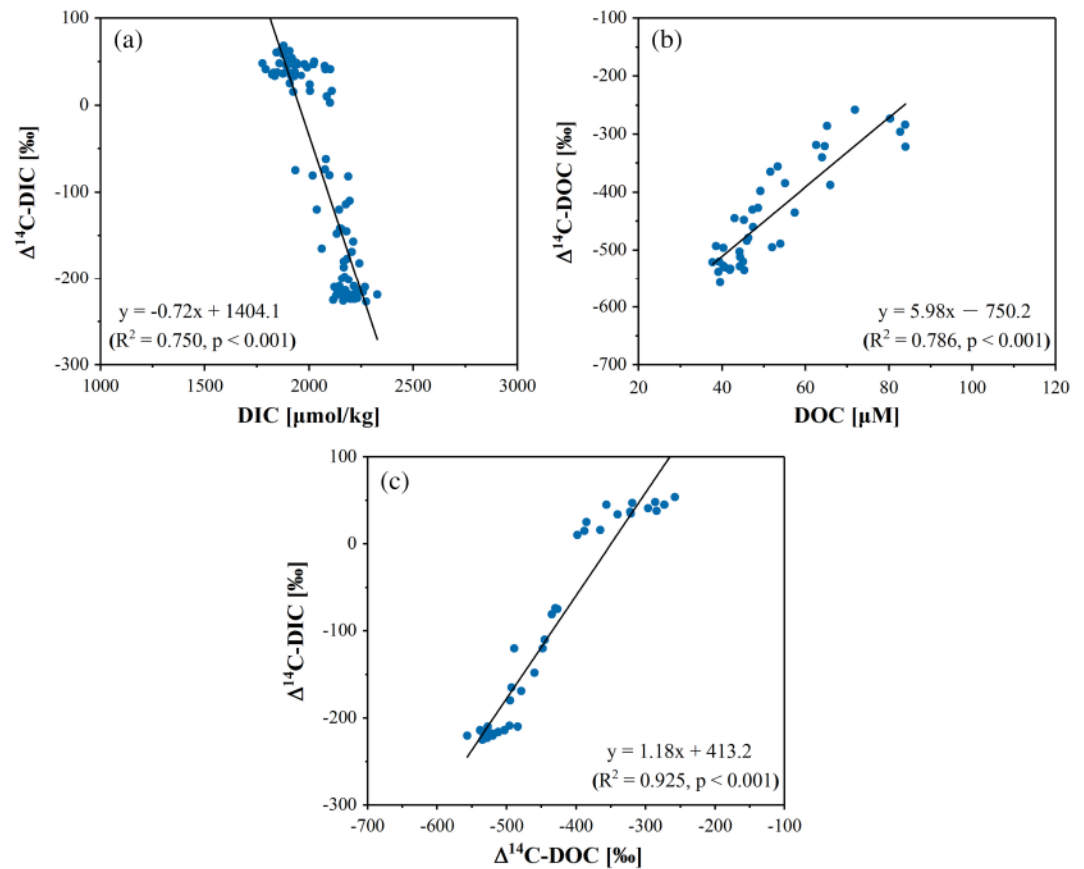
Figure 7. (a) DIC concentrations and Δ^{14}C-DIC, (b) DOC concentrations and Δ^{14}C-DOC, and (c) Δ^{14}C-DOC and Δ^{14}C-DIC correlation plots for samples collected from the stations in the SCS and NWP. The solid black lines denote linear regressions fit to the data.

4.3. Application of the Keeling Plot in the SCS

Keeling plot analyses that identify the Δ^{14}C value of an excess component added to a background pool have been performed on both oceanic DIC and DOC depth profiles to discern the consistency with solution-based two-component mixing (Beaupré & Aluwihare, 2010). We examined the Keeling plots of DIC and DOC for the SCS, as shown in Figure 8.

The Keeling plot of DIC is linear and possessed a high coefficient with $R^2 = 0.66$ ($p < 0.001$, $n = 63$), as determined by Model II regression (geometric mean regression) (Figure 8a), confirming that the main controls on the observed distributions of DIC and Δ^{14}C-DIC were hydrodynamic mixing processes within the SCS. The DIC Keeling plot in the SCS (slope $= 3.5 \times 10^6$) is consistent with those obtained in the Kuroshio Extension region and the eastern NP (4×10^6 and 4.29×10^6, respectively), confirming that DIC concentrations and Δ^{14}C-DIC can be used as conservative tracers of water mass movement and water parcel homogenization (Beaupré & Aluwihare, 2010; Ding et al., 2018), and thus the distribution of Δ^{14}C-DIC could be predicted by the solution mixing model in the SCS. If we use the average value of 49‰ for Δ^{14}C-DIC of the Kuroshio water mass in the upper 500 m depth (Stations C05 and C08) and −218‰ for Δ^{14}C-DIC of the NP deep water at depths deeper than 1,500 m (Figure 8a and Table S2), we calculated that 46–82% of the NP deep water could have been upwelled and mixed with Kuroshio water in the upper 250–700 m depth based on the mass balance, thus resulting in the observed Δ^{14}C-DIC profiles in the SCS, suggesting that water mixing in the upper 800 m depth in the basin of the SCS is quite dynamic and the ventilation by water exchange is more rapid in the upper 800 m depth than that in the deep basin water.
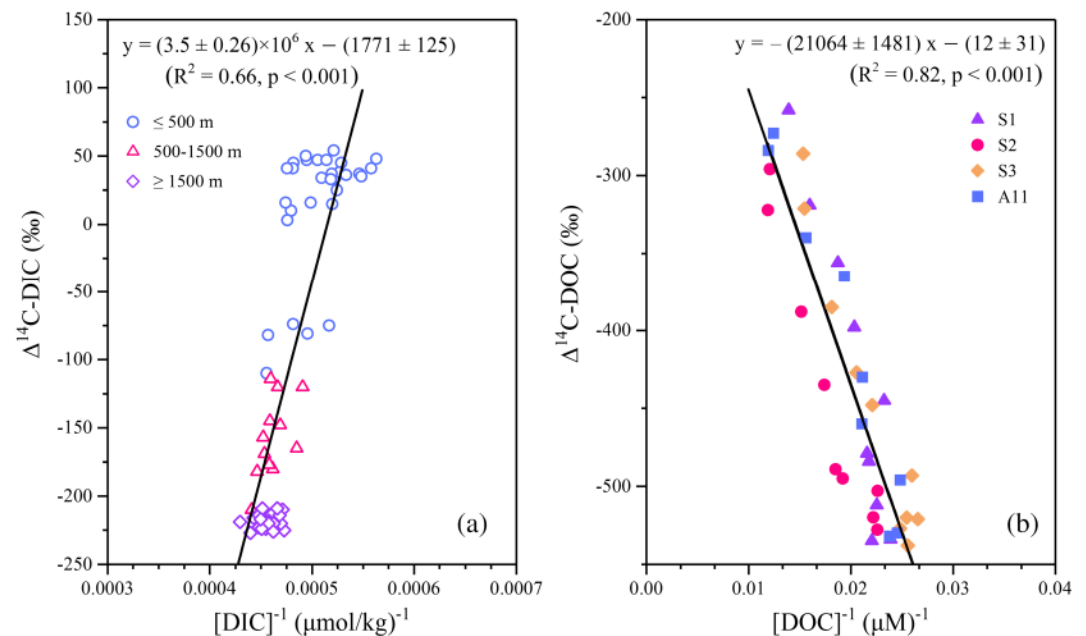
Figure 8. (a) DIC and (b) DOC Keeling plots of measurements from six and four stations, respectively, in the SCS. A Model II regression (geometric mean regression) was used to estimate the slope and intercept of the regression line. The black lines indicate the Model II geometric mean regression of all points.

The DOC Keeling plot (Figure 8b) was also linear and possessed an even higher coefficient of determination ($R^2 = 0.82$, $p < 0.001$, $n = 39$) in all depth profiles. This seemingly linear relationship indicates that the Δ^{14}C-DOC value of an excess component added to a background pool (Mortazavi & Chanton, 2004). The intercepts of the DOC Keeling plots in the Pacific (73–188‰) and Atlantic (10–117‰) were similar to the surface water Δ^{14}C-DIC values in both oceans, suggesting that the excess DOC (DOC_{xs}) component originated from recent production in the surface ocean and was further rapidly transported to mesopelagic waters (Beaupré & Aluwihare, 2010; Druffel et al., 2016; Mortazavi & Chanton, 2004). However, the Keeling plot of the SCS DOC data revealed an intercept (-12 ± 31‰) that was lower than the surface Δ^{14}C-DIC values (42 ± 7‰). This could imply that the surface production is not the only source for DOC_{xs} component in the deep SCS. The DOC_{xs} could be a mixed component derived from recent production, old DOC from land, and recalcitrant DOC in the deep water. As a large semienclosed marginal sea in the tropical NWP, enhanced diapycnal mixing and vertical motion could be the main factors influencing the hydrological characteristics and DOC distribution in the SCS basin, which could be different from those in the open oceans.

5. Conclusions

Our combined radiocarbon, stable carbon isotope, and concentration measurements of DIC and DOC in the SCS revealed the nature of rapid carbon cycling in the SCS. We drew the following conclusions from this study:

1. The concentrations of DIC ranged from 1,776 to 2,328 μmol kg^{-1}, low at the surface and increasing with depth. The Δ^{14}C-DIC values varied in the range of -227‰ to 68‰, high at the surface and decreasing rapidly with depth to ~1,500 m, then remaining constant. The large variability in the Δ^{14}C signature in the upper 1,000 m between the SCS and NWP reflects the different water masses and mixing dynamics. The relatively lower Δ^{14}C-DIC values for the stations in the upper 250–700 m depth in the SCS were primarily controlled by intensified vertical mixing, which upwelled the NP deep water with low Δ^{14}C-DIC values in the proportion of 46–82% and mixed with the Kuroshio water in the upper layer. In contrast, the small difference in Δ^{14}C-DIC values in the water deeper than 1,500 m confirmed the rapid water exchange through the Luzon Strait and good water mixing in the basin of the SCS.

2. The concentrations and $\Delta^{14}C$ values of DOC in the SCS showed typical vertical distribution patterns in the open ocean, with ranges of 38 to 95 μM and −557‰ to −258‰, respectively. The relatively low $\Delta^{14}C$-DOC values in the SCS upper layer water (100–250 m) indicated vertical mixing of deep waters with lower DOC $\Delta^{14}C$ upwelled to the surface. However, the similarity of $\Delta^{14}C$-DOC values below a depth of 1,500 m between the SCS and central NP suggested that DOC was transported with the inflow across the Luzon Strait from the NWP and well mixed in the deep SCS.

3. Together with the carbon isotope and concentration measurements of DIC and DOC in the SCS, the dynamics of DIC and DOC in the deep SCS are mainly controlled by hydrodynamic processes, such as diffusive mixing and intensified vertical motion. In addition, the much older ages of DOC ^{14}C than DIC (by 3,900 ± 248 years) implied that a large fraction of deep DOC has been cycled for a longer time than DIC in the deep SCS.

References

Beaupré, S. R., & Aluwihare, L. (2010). Constraining the 2-component model of marine dissolved organic radiocarbon. *Deep Sea Research Part II: Topical Studies in Oceanography*, 57(16), 1494–1503. https://doi.org/10.1016/j.dsr2.2010.02.017

Beaupré, S. R., & Druffel, E. R. M. (2009). Constraining the propagation of bomb-radiocarbon through the dissolved organic carbon (DOC) pool in the Northeast Pacific Ocean. *Deep Sea Research Part I: Oceanographic Research Papers*, 56(10), 1717–1726. https://doi.org/10.1016/j.dsr.2009.05.008

Bercovici, S. K., & Hansell, D. A. (2016). Dissolved organic carbon in the deep Southern Ocean: Local versus distant controls. *Global Biogeochemical Cycles*, 30(2), 350–360. https://doi.org/10.1002/2015GB005252

Broecker, W. S., Patzert, W. C., Toggweiler, J. R., & Stuiver, M. (1986). Hydrography, chemistry, and radioisotopes in the Southeast Asian basins. *Journal of Geophysical Research*, 91(C12), 14,345–14,354. https://doi.org/10.1029/JC091iC12p14345

Broecker, W. S., Peng, T.-H., Ostlund, G., & Stuiver, M. (1985). The distribution of bomb radiocarbon in the ocean. *Journal of Geophysical Research*, 90(C4), 6953–6970. https://doi.org/10.1029/JC090iC04p06953

Cao, Z., Dai, M., Zheng, N., Wang, D., Li, Q., Zhai, W., et al. (2011). Dynamics of the carbonate system in a large continental shelf system under the influence of both a river plume and coastal upwelling. *Journal of Geophysical Research*, 116, G02010. https://doi.org/10.1029/2010JG001596

Carlson, C. A., Ducklow, H. W., & Michaels, A. F. (1994). Annual flux of dissolved organic carbon from the euphotic zone in the northwestern Sargasso Sea. *Nature*, 371(6496), 405–408. https://doi.org/10.1038/371405a0

Carlson, C. A., Hansell, D. A., Nelson, N. B., Siegel, D. A., Smethie, W. M., Khatiwala, S., et al. (2010). Dissolved organic carbon export and subsequent remineralization in the mesopelagic and bathypelagic realms of the North Atlantic basin. *Deep Sea Research Part II*, 57(16), 1433–1445. https://doi.org/10.1016/j.dsr2.2010.02.013

Chen, C. T. A., & Huang, M. H. (1996). A mid-depth front separating the South China Sea water and the Philippine sea water. *Journal of Oceanography*, 52(1), 17–25. https://doi.org/10.1007/BF02236530

Chen, C. T. A., Wang, S. L., Wang, B. J., & Pai, S. C. (2001). Nutrient budgets for the South China Sea basin. *Marine Chemistry*, 75(4), 281–300. https://doi.org/10.1016/S0304-4203(01)00041-X

Dai, M., Cao, Z., Guo, X., Zhai, W., Liu, Z., Yin, Z., et al. (2013). Why are some marginal seas sources of atmospheric CO_2? *Geophysical Research Letters*, 40(10), 2154–2158. https://doi.org/10.1002/grl.50390

Dai, M., Meng, F., Tang, T., Kao, S.-J., Lin, J., Chen, J., et al. (2009). Excess total organic carbon in the intermediate water of the South China Sea and its export to the North Pacific. *Geochemistry, Geophysics, Geosystems*, 10, Q12002. https://doi.org/10.1029/2009GC002752

Dai, M., Gan, J., Han, A., Kung, H. S., & Yin, Z. (2014). Physical dynamics and biogeochemistry of the Pearl River plume. In T. S. Bianchi, M. Allison, & W.-J. Cai (Eds.), *Biogeochemical Dynamics at Major River-Coastal Interfaces. Linkages with Global Change* (pp. 321–352). New York: Cambridge University Press.

Ding, L., Ge, T., Gao, H., Luo, C., Xue, Y., Druffel, E. R. M., & Wang, X. (2018). Large variability of dissolved inorganic radiocarbon in the Kuroshio Extension of the northwest North Pacific. *Radiocarbon*, 60(2), 691–704. https://doi.org/10.1017/RDC.2017.143

Druffel, E. R. M., & Bauer, J. E. (2000). Radiocarbon distributions in Southern Ocean dissolved and particulate organic matter. *Geophysical Research Letters*, 27(10), 1495–1498. https://doi.org/10.1029/1999GL002398

Druffel, E. R. M., Williams, P. M., Bauer, J. E., & Ertel, J. R. (1992). Cycling of dissolved and particulate organic matter in the open ocean. *Journal of Geophysical Research*, 97(C10), 15,639–15,659. https://doi.org/10.1029/92JC01511

Druffel, E. R. M., Bauer, J. E., Griffin, S., Beaupré, S. R., & Hwang, J. (2008). Dissolved inorganic radiocarbon in the North Pacific Ocean and Sargasso Sea. *Deep Sea Research Part I: Oceanographic Research Papers*, 55(4), 451–459. https://doi.org/10.1016/j.dsr.2007.12.007

Druffel, E. R. M., & Griffin, S. (2015). Radiocarbon in dissolved organic carbon of the South Pacific Ocean. *Geophysical Research Letters*, 42(10), 4096–4101. https://doi.org/10.1002/2015GL063764

Druffel, E. R. M., Griffin, S., Coppola, A. I., & Walker, B. D. (2016). Radiocarbon in dissolved organic carbon of the Atlantic Ocean. *Geophysical Research Letters*, 43(10), 5279–5286. https://doi.org/10.1002/2016GL068746

Druffel, E. R. M., Griffin, S., Wang, N., Garcia, N. G., McNichol, A. P., Key, R. M., & Walker, B. D. (2019). Dissolved organic radiocarbon in the Central Pacific Ocean. *Geophysical Research Letters*, 46(10), 5396–5403. https://doi.org/10.1029/2019GL083149

Du, C., Liu, Z., Dai, M., Kao, S. J., Cao, Z., Zhang, Y., et al. (2013). Impact of the Kuroshio intrusion on the nutrient inventory in the upper northern South China Sea: Insights from an isopycnal mixing model. *Biogeosciences*, 10(10), 6419–6432. https://doi.org/10.5194/bg-10-6419-2013

Follett, C. L., Repeta, D. J., Rothman, D. H., Xu, L., & Santinelli, C. (2014). Hidden cycle of dissolved organic carbon in the deep ocean. *Proceedings of the National Academy of Sciences*, 111(47), 16,706–16,711. https://doi.org/10.1073/pnas.1407445111

Fukasawa, M., Kawano, T., Murata, A., Shibata, F., Kitada, M., Ohama, T., & Ishikawa, Y. (2005). Carbon dioxide, hydrographic, and chemical data obtained during the R/V *Mirai* Repeat Hydrography Cruise in the Pacific Ocean: CLIVAR CO_2 Section P10_2005 (25 May - 2 July, 2005). https://cdiac.ornl.gov/ftp/oceans/CLIVAR/P10_2005.data/. Carbon Dioxide Information Analysis Center, Oak Ridge National Laboratory, US Department of Energy, Oak Ridge, Tennessee. https://doi.org/10.3334/CDIAC/otg.CLIVAR_P10_2005

Gao, P., Zhou, L., Liu, K., & Xu, X. (2019). Radiocarbon in the maritime air and sea surface water of the South China Sea. *Radiocarbon*, *61*(2), 461–472. https://doi.org/10.1017/RDC.2018.100

Ge, T., Wang, X., Zhang, J., Luo, C., & Xue, Y. (2016). Dissolved inorganic radiocarbon in the Northwest Pacific continental margin. *Radiocarbon*, *58*(3), 517–529. https://doi.org/10.1017/RDC.2016.23

Gong, G. C., Liu, K. K., Liu, C. T., & Pai, S. C. (1992). The chemical hydrography of the South China Sea west of Luzon and a comparison with the West Philippine Sea. *Terrestrial, Atmospheric and Oceanic Sciences*, *3*(4), 587–602. https://doi.org/10.3319/TAO.1992.3.4.587(O)

Graven, H. D., Gruber, N., Key, R., Khatiwala, S., & Giraud, X. (2012). Changing controls on oceanic radiocarbon: New insights on shallow-to-deep ocean exchange and anthropogenic CO_2 uptake. *Journal of Geophysical Research*, *117*, C10005. https://doi.org/10.1029/2012JC008074

Gruber, N. (2011). Warming up, turning sour, losing breath: Ocean biogeochemistry under global change. *Philosophical Transactions of the Royal Society A*, *369*(1943), 1980–1996. https://doi.org/10.1098/rsta.2011.0003

Hansell, D. A., & Carlson, C. A. (2001). Marine dissolved organic matter and the carbon cycle. *Oceanography*, *14*(4), 41–49. https://doi.org/10.5670/oceanog.2001.05

Hansell, D. A., & Carlson, C. A. (2013). Localized refractory dissolved organic carbon sinks in the deep ocean. *Global Biogeochemical Cycles*, *27*(3), 705–710. https://doi.org/10.1002/gbc.20067

Hansell, D. A., Carlson, C. A., Repeta, D. J., & Schlitzer, R. (2009). Dissolved organic matter in the ocean: A controversy stimulates new insights. *Oceanography*, *22*(4), 202–211. https://doi.org/10.5670/oceanog.2009.109

Hu, J., Kawamura, H., Hong, H., & Qi, Y. (2000). A review on the currents in the South China Sea: Seasonal circulation, South China Sea warm current and Kuroshio intrusion. *Journal of Oceanography*, *56*(6), 607–624. https://doi.org/10.1023/A:1011117531252

Hua, Q., Barbetti, M., & Rakowski, A. Z. (2013). Atmospheric radiocarbon for the period 1950–2010. *Radiocarbon*, *55*(4), 2059–2072. https://doi.org/10.2458/azu_js_rc.v55i2.16177

Hung, J. J., Wang, S. M., & Chen, Y. L. (2007). Biogeochemical controls on distributions and fluxes of dissolved and particulate organic carbon in the northern South China Sea. *Deep Sea Research Part II: Topical Studies in Oceanography*, *54*(14–15), 1486–1503. https://doi.org/10.1016/j.dsr2.2007.05.006

Key, R. M. (1996). WOCE Pacific Ocean radiocarbon program. *Radiocarbon*, *38*(3), 415–423. https://doi.org/10.1017/S003382220003006X

Key, R. M., Kozyr, A., Sabine, C. L., Lee, K., Wanninkhof, R., Bullister, J. L., et al. (2004). A global ocean carbon climatology: Results from Global Data Analysis Project (GLODAP). *Global Biogeochemical Cycles*, *18*, GB4031. https://doi.org/10.1029/2004GB002247

Key, R. M., Quay, P. D., Jones, G. A., McNichol, A. P., Von Reden, K. F., & Schneider, R. J. (1996). WOCE AMS Radiocarbon I: Pacific Ocean results (P6, P16 and P17). *Radiocarbon*, *38*(3), 425–518. https://doi.org/10.1017/S0033822200030071

Key, R. M., Quay, P. D., Schlosser, P., McNichol, A. P., von Reden, K. F., Schneider, R. J., et al. (2002). WOCE Radiocarbon IV: Pacific Ocean results; P10, P13N, P14C, P18, P19 & S4P. *Radiocarbon*, *44*(1), 239–392. https://doi.org/10.1017/S0033822200064845

Lan, J., Zhang, N., & Wang, Y. (2013). On the dynamics of the South China Sea deep circulation. *Journal of Geophysical Research: Oceans*, *118*, 1206–1210. https://doi.org/10.1002/jgrc.20104

Levin, I., Kromer, B., & Hammer, S. (2013). Atmospheric $\Delta^{14}CO_2$ trend in Western European background air from 2000 to 2012. *Tellus Series B: Chemical and Physical Meteorology*, *65*(1), 20092. https://doi.org/10.3402/tellusb.v65i0.20092

Liu, Q., Kaneko, A., & Jilan, S. (2008). Recent progress in studies of the South China Sea circulation. *Journal of Oceanography*, *64*(5), 753–762. https://doi.org/10.1007/s10872-008-0063-8

McNichol, A. P., & Aluwihare, L. I. (2007). The power of radiocarbon in biogeochemical studies of the marine carbon cycle: Insights from studies of dissolved and particulate organic carbon (DOC and POC). *Chemical Reviews*, *107*(2), 443–466. https://doi.org/10.1021/cr050374g

McNichol, A. P., & Jones, G. A. (1991). Measuring ^{14}C in seawater $\sum CO_2$ by accelerator mass spectrometry. In T. Joyce, C. Corry, & M. Stalcup (Eds.), *World Ocean Circulation Experiment Operations Manual* (pp. >71). Massachusetts: Woods Hole, WHPO Publication 90-1.

McNichol, A. P., Jones, G. A., Hutton, D. L., Gagnon, A. R., & Key, R. M. (1994). The rapid preparation of seawater $\sum CO_2$ for radiocarbon analysis at the National Ocean Sciences AMS Facility. *Radiocarbon*, *36*(2), 237–246. https://doi.org/10.1017/S0033822200040522

McNichol, A. P., Schneider, R. J., von Reden, K. F., Gagnon, A. R., Elder, K. L., Nosams, K., & R. M., & Quay, P. D. (2000). Ten years after—The WOCE AMS radiocarbon program. *Nuclear Instruments and Methods in Physics Research Section B: Beam Interactions with Materials and Atoms*, *172*(1–4), 479–484. https://doi.org/10.1016/S0168-583X(00)00093-8

Mortazavi, B., & Chanton, J. P. (2004). Use of Keeling plots to determine sources of dissolved organic carbon in nearshore and open ocean systems. *Limnology and Oceanography*, *49*(1), 102–108. https://doi.org/10.4319/lo.2004.49.1.0102

Nan, F., Xue, H., & Yu, F. (2015). Kuroshio intrusion into the South China Sea: A review. *Progress in Oceanography*, *137*(Part A), 314–333. https://doi.org/10.1016/j.pocean.2014.05.012

Qu, T., Girton, J. B., & Whitehead, J. A. (2006). Deepwater overflow through Luzon Strait. *Journal of Geophysical Research*, *111*, C01002. https://doi.org/10.1029/2005jc003139

Schlitzer, R. (2017). Ocean Data View 4. http://odv.awi.de

Sharp, J. H., Benner, R., Bennett, L., Carlson, C. A., Fitzwater, S. E., Peltzer, E. T., & Tupas, L. M. (1995). Analyses of dissolved organic carbon in seawater: The JGOFS EqPac methods comparison. *Marine Chemistry*, *48*(2), 91–108. https://doi.org/10.1016/0304-4203(94)00040-K

Shu, Y., Xue, H., Wang, D., Chai, F., Xie, Q., Yao, J., & Xiao, J. (2014). Meridional overturning circulation in the South China Sea envisioned from the high-resolution global reanalysis data GLBa0.08. *Journal of Geophysical Research, Oceans*, *119*(5), 3012–3028. https://doi.org/10.1002/2013JC009583

Stuiver, M., & Polach, H. A. (1977). Discussion reporting of ^{14}C data. *Radiocarbon*, *19*(3), 355–363. https://doi.org/10.1017/S0033822200003672

Stuiver, M., Quay, P. D., & Östlund, H. G. (1983). Abyssal water carbon-14 distribution and the age of the world oceans. *Science*, *219*(4586), 849–851. https://doi.org/10.1126/science.219.4586.849

Su, J. (2004). Overview of the South China Sea circulation and its influence on the coastal physical oceanography outside the Pearl River Estuary. *Continental Shelf Research*, *24*(16), 1745–1760. https://doi.org/10.1016/j.csr.2004.06.005

Tian, J., & Qu, T. (2012). Advances in research on the deep South China Sea circulation. *Chinese Science Bulletin*, *57*(24), 3115–3120. https://doi.org/10.1007/s11434-012-5269-x

Tian, J., Yang, Q., Liang, X., Xie, L., Hu, D., Wang, F., & Qu, T. (2006). Observation of Luzon Strait transport. *Geophysical Research Letters*, *33*, L19607. https://doi.org/10.1029/2006gl026272

Tian, J. W., Yang, Q. X., & Zhao, W. (2009). Enhanced diapycnal mixing in the South China Sea. *Journal of Physical Oceanography*, *39*(12), 3191–3203. https://doi.org/10.1175/2009JPO3899.1

Wakita, M., Watanabe, S., Murata, A., Tsurushima, N., & Honda, M. (2010). Decadal change of dissolved inorganic carbon in the subarctic western North Pacific Ocean. *Tellus B*, *62*(5), 608–620. https://doi.org/10.1111/j.1600-0889.2010.00476.x

Wang, D., Xiao, J., Shu, Y., Xie, Q., Chen, J., & Wang, Q. (2016). Progress on deep circulation and meridional overturning circulation in the South China Sea. *Science China Earth Sciences*, *59*(9), 1827–1833. https://doi.org/10.1007/s11430-016-5324-6

Wang, P., & Li, Q. (2009). Oceanographical and geological background. In P. Wang & Q. Li (Eds.), *The South China Sea: Paleoceanography and Sedimentology* (pp. 25–73). Netherlands: Springer. https://doi.org/10.1007/978-1-4020-9745-4_2

Williams, P. M., & Druffel, E. R. M. (1987). Radiocarbon in dissolved organic matter in the central North Pacific Ocean. *Nature*, *330*(6145), 246–248. https://doi.org/10.1038/330246a0

Winn, C. D., Li, Y.-H., Mackenzie, F. T., & Karl, D. M. (1998). Rising surface ocean dissolved inorganic carbon at the Hawaii Ocean Time-series site. *Marine Chemistry*, *60*(1–2), 33–47. https://doi.org/10.1016/S0304-4203(97)00085-6

Wu, K., Dai, M., Chen, J., Meng, F., Li, X., Liu, Z., et al. (2015). Dissolved organic carbon in the South China Sea and its exchange with the Western Pacific Ocean. *Deep Sea Research Part II: Topical Studies in Oceanography*, *122*, 41–51. https://doi.org/10.1016/j.dsr2.2015.06.013

Xue, Y., Ge, T., & Wang, X. (2015). An effective method of UV-oxidation of dissolved organic carbon in natural waters for radiocarbon analysis by accelerator mass spectrometry. *Journal of Ocean University of China*, *14*(6), 989–993. https://doi.org/10.1007/s11802-015-2935-z

Zigah, P. K., McNichol, A. P., Xu, L., Johnson, C., Santinelli, C., Karl, D. M., & Repeta, D. J. (2017). Allochthonous sources and dynamic cycling of ocean dissolved organic carbon revealed by carbon isotopes. *Geophysical Research Letters*, *44*(5), 2407–2415. https://doi.org/10.1002/2016GL071348